Biogeosciences Discuss., 11, 9299–9340, 2014
www.biogeosciences-discuss.net/11/9299/2014/
doi:10.5194/bgd-11-9299-2014

Biogeosciences Discussions
Open Access

Performance evaluation of ocean color satellite models for deriving accurate chlorophyll estimates in the Gulf of Saint Lawrence

M. Montes-Hugo[1], H. Bouakba[1], and R. Arnone[2]

[1]Institut de Sciences de la Mer de Rimouski, Université du Québec à Rimouski, 310 Alleé des Ursulines, Office P-216, G5L 3A1, Rimouski, Québec, Canada
[2]University of Southern Mississippi, Department of Marine Science, 1020 Balch Blvd, Stennis Space Center, MS 39529, USA

Received: 23 April 2014 – Accepted: 29 April 2014 – Published: 17 June 2014

Correspondence to: M. Montes-Hugo (martinalejandro_montes@uqar.ca)

Published by Copernicus Publications on behalf of the European Geosciences Union.

Abstract

The understanding of phytoplankton dynamics in the Gulf of the Saint Lawrence (GSL) is critical for managing major fisheries off the Canadian East coast. In this study, the accuracy of two atmospheric correction techniques (NASA standard algorithm, SA, and Kuchinke's spectral optimization, KU) and three ocean color inversion models (Carder's empirical for SeaWiFS (Sea-viewing Wide Field-of-View Sensor), EC, Lee's quasi-analytical, QAA, and Garver- Siegel-Maritorena semi-empirical, GSM) for estimating the phytoplankton absorption coefficient at 443 nm ($a_{ph}(443)$) and the chlorophyll concentration (chl) in the GSL is examined. Each model was validated based on SeaWiFS images and shipboard measurements obtained during May of 2000 and April 2001. In general, $a_{ph}(443)$ estimates derived from coupling KU and QAA models presented the smallest differences with respect to in situ determinations as measured by High Pressure liquid Chromatography measurements (median absolute bias per cruise up to 0.005, RMSE up to 0.013). A change on the inversion approach used for estimating $a_{ph}(443)$ values produced up to 43.4 % increase on prediction error as inferred from the median relative bias per cruise. Likewise, the impact of applying different atmospheric correction schemes was secondary and represented an additive error of up to 24.3 %. By using SeaDAS (SeaWiFS Data Analysis System) default values for the optical cross section of phytoplankton (i.e., $a^*_{ph}(443) = a_{ph}(443)/\mathrm{chl} = 0.056\,\mathrm{m^2\,mg^{-1}}$), the median relative bias of our chl estimates as derived from the most accurate space-borne $a_{ph}(443)$ retrievals and with respect to in situ determinations increased up to 29 %.

1 Introduction

The spatial and temporal variability of productivity of aquatic systems is mainly driven by phytoplankton abundance. Also, phytoplankton has a major impact modulating cli-

mate (e.g., production of aerosols, air–water exchange of gases) (Charlson et al., 1987) and ocean currents (e.g., heat within the upper mixed layer) (Morel and Antoine, 1994).

The chlorophyll *a* concentration (chl) is the main photosynthetic pigment of phytoplankton, thus it is commonly used as a proxy of phytoplankton abundance. Likewise, chlorophyll *a* is a major light absorbing component in coastal and oceanic waters, and is related to the phytoplankton (a_{ph}) and total (a) absorption coefficient as follows

$$a_{ph}(\lambda) = \text{chl}\, a^*_{ph}(\lambda) \quad (1)$$

$$a(\lambda) = a_w(\lambda) + a_d(\lambda) + a_{CDOM}(\lambda) + a_{ph}(\lambda) \quad (2)$$

where λ is the light wavelength within the visible spectral range (i.e., 400–700 nm), subscripts w, d and CDOM represent the water, detritus, and chromophoric dissolved organic matter contributions, respectively (Table 1). Notice that "water" contribution may have a variable salinity encompassing fresh, brackish and marine waters but this effect on a_w can be neglected (Levender et al., 2005). The magnitude of a^*_{ph} (i.e., the absorption cross section of phytoplankton) is influenced by the proportion of photoprotective pigments, the photo-acclimation state, and the cell size spectra of phytoplankton (Bricaud et al., 2004). The last two parameters are usually grouped as part of the "packaging effect" or the intracellular change on pigment concentration and location due to variations of photosynthetically available radiation (i.e., wavelengths between 400 and 700 nm).

The mapping of chl over large and dynamic environments is prone to important spatial aliasing when pigment samples are based on shipboard surveys. This limitation is absent if chl fields are derived from synoptic measurements obtained from spaceborne ocean color sensors. However, the accuracy of satellite-derived chl estimates or chl-related parameters (e.g., $a_{ph}(\lambda_0)$, where λ_0 is the centered band at 443 nm and corresponds to the maximum absorption peak of phytoplankton at 440 nm) may be compromised if two processing steps are not carefully addressed: the atmospheric correction and the discrimination of water optical components including the phytoplankton.

A critical task for deriving accurate water leaving radiance (L_w) values in waters presenting different optical properties is the removal of atmospheric constituents affecting the radiance reaching the satellite detector. The classic atmospheric correction approach is based on the "dark pixel" assumption in the near-infrared (NIR) spectral range (i.e., λ = 700–1000 nm) (Gordon and Wang, 1994). In other words, the proportion of TOA (Top-Of-the Atmosphere) attributed to L_w is zero at NIR wavelengths. Although useful in relatively clear waters, this approximation is not generally valid when the concentration of suspended solids is above 1 g m^{-3} (Levender et al., 2005). To avoid these caveats, more recent atmospheric correction parameterizations include results from underwater light models to constraint atmospheric parameters such as aerosol concentration and type (Kuchinke et al., 2009; Bailey et al., 2010).

In general, as the contribution of non-algal components to inherent optical properties (IOPs) (i.e., those only changing according to the characteristics of the optical constituents) increases, the spectral overlap between optical constituents becomes more severe resulting a major overestimation (e.g., mineral-rich waters, Balch et al., 1989; Wozniak and Stramski, 2004) or underestimation (e.g., CDOM-dominated waters, Montes-Hugo et al., 2005) of satellite-derived chl values. These deviations may be in part reduced by increasing the spectral resolution (i.e., more and/or narrower radiometric bands) of ocean color imagers. However, this improvement may not help if the method used for computing IOPs including those from phytoplankton (hereafter "inversion model") is not very accurate.

The reconstruction of IOPs from apparent optical properties (AOPs) (i.e., those depending on IOPs and the geometry of the light field) can be achieved using the following equation derived from the radiative-transfer theory (Gordon et al., 1988):

$$\text{nL}_w(\lambda) = t_{a-w} F_o(\lambda)/n_w^2 \sum_{i=1}^{2} g_i \left\{ \frac{b_b(\lambda)}{(b_b(\lambda) + a(\lambda))} \right\}^i \quad (3)$$

$$R_{rs}(\lambda) = \text{nL}_w(\lambda)/F_o(\lambda) \quad (4)$$

where nL_w is the normalized L_w with respect to the sun altitude and sensor viewing geometry, t_{a-w} is the sea–air transmission factor, $F_o(\lambda)$ is the mean extraterrestrial solar irradiance, n_w is the refractive index of the water, $R_{rs}(\lambda)$ is the remote sensing reflectance, t_{a-w}/n_w^2 approximates to 1, and g's values can be obtained for averaged or specific illumination and viewing conditions (Morel et al., 2002).

In general, inversion models are input with $nL_w(\lambda)$ or $R_{rs}(\lambda)$ measurements and compute chl or $a_{ph}(443)$ values in a direct (i.e., based on $nL_w(\lambda)$ or $R_{rs}(\lambda)$ functionalities) or indirect way (i.e., from a estimates, Eq. 2), and they can be grouped as: empirical, semi-empirical and pattern-recognition. A good description of each approach along its performance for estimating IOPs is summarized in the report 5 of the International Ocean Color Coordinating Group (Lee, 2006). Empirical models are commonly developed with R_{rs} ratios and are based on regression functions. Semi-empirical models require analytics expressions relating IOPs and AOPs, mathematical constraints and non-linear regression optimizations techniques. Lastly, pattern recognition methods are constructed based on rules (e.g., neural networks) or similarity indices (e.g., maximum likelihood).

In addition to the aforementioned source errors, the accuracy of satellite retrievals of chl or $a_{ph}(443)$ is also influenced by two factors: uncertainties on $a^*_{ph}(\lambda)$ and differences in terms of time-space scales between IOPs and satellite measurements. Regarding the first factor, it is a known fact that an inadequate selection of spectral a^*_{ph} curves may result in large deviations on spaceborne chl estimates with respect to field determinations (Gilerson et al., 2010). Unfortunately and despite some interesting attempts (Carder et al., 1999), no satisfactory models exist in the literature to date for estimating $a^*_{ph}(\lambda)$ based on remote sensing observations. The second factor described above introduces uncertainty when comparisons between remote sensing and field measurements are performed in environments where the scales of variability of chl are smaller than the sensor footprint and/or the time interval between the satellite and in situ data. Notice that the bias associated to the spatial variability is also attributed to the vertical

variability of IOPs within the first optical depth (i.e., depth at which 95 % of the water leaving radiance reaching the satellite sensor originates, Gordon and McCluney, 1975).

The Gulf of the Saint Lawrence (GSL) is a very productive system supporting major fisheries off the Atlantic Canadian coast (Runge et al., 1999; Koeller et al., 2009). The GSL ecosystem is strongly influenced by summer-fall storms and important interannual and seasonal variations on freshwater discharge (Fuentes-Yaco et al., 1997a; Nieke et al., 1997; Le Fouest et al., 2005). These oceanographic conditions create a complex underwater light field resulting from combining estuarine and oceanic water parcels having different proportion of optical components (Nieke et al., 1997). In this context, the development of satellite ocean color algorithms for accurate mapping of chl in the GSL is challenging and explains the limited success of past investigations using traditional inversion techniques based on blue-green ratios (Fuentes-Yaco et al., 1997b). Another complication in the GSL for deriving chl from satellites is the change of phytoplankton photo-physiology and size structure with respect to the hydrological regime. These alterations produce modifications on a^*_{ph} (Roy et al., 2008) and biases on subsequent space-based estimates of chl that need to be addressed for improving the accuracy of chl predictions made by biogeochemical models coupled to circulation (Le Fouest et al., 2005). Lastly, it is unknown how each uncertainty (i.e., atmospheric correction, IOPs inversion approach, variability of phytoplankton photoacclimation) contributes to the total error on satellite chl estimates over the GSL.

The aim of this study is to quantify the accuracy of different atmospheric correction and inversion models for estimating $a_{ph}(443)$ and chl in surface waters of the GSL. Also of interest, is to examine the importance of different sources of errors on satellite retrievals. It is hypothesized that accuracy of semi-empirical inversion models for estimating spaceborne $a_{ph}(443)$ values will improve with respect to empirical algorithms when the river discharge into the GSL increases and viceversa. This pattern is mainly justified by the fact that optically complex waters are more prevalent when the GLS have a greater contribution of estuarine waters characterized by IOPs that are no co-

varying with phytoplankton. In this case, semi-empirical inversions can perform better than empirical approaches for discriminating a greater diversity of optical signatures.

The results and discussion are divided in three major sections. In the first section, we analyze and rank the performance of two atmospheric correction techniques and three inversion models of IOPs for estimating $a_{ph}(443)$ values in surface waters of the GSL and during spring of 2000 and 2001. In the second section, bias of $a_{ph}(443)$ space-borne estimates is examined with respect to the distance to the coast and the presence of different hydrographic features. Lastly, the influence of $a^*_{ph}(443)$ on satellite-derived $a_{ph}(443)$ uncertainties is evaluated.

2 Methods

2.1 Study area

The GSL is a large subarctic marginal sea with an average cross section of 500 km (Fig. 1). The GSL basin is a meeting point between estuarine waters coming from the Saint Lawrence River and more saline waters coming from the North Atlantic Ocean (Koutitonsky and Budgen, 1991). The GSL is relatively shallow (e.g., up to 50 m depth in the Magdalen shallows), thus the main water exchange occur along the main trough also known as the Laurentien channel. The freshwater supply into the Gulf is substantial and highly variable due to seasonal runnof and melting of sea ice (Le Fouest et al., 2005). The general circulation over the GSL is mainly driven by tides and synoptic winds, and is characterized by a complex hydrography that includes fronts, gyres, eddies and coastal upwelling (Koutitonsky and Budgen, 1991; Saucier et al., 2003; Josenhans, 2007) (Fig. A1).

The distribution of phytoplankton over the GSL is very heterogeneous and it is strongly linked to regional circulation patterns (de Lafontaine et al., 1991; Le Fouest et al., 2005). Indeed, an important feature modulating the phytoplankton growth over shallow locations of the SW GSL is the Gaspé Current, a baroclinic jet forced by the

main estuarine flow (Savenkoff et al., 2001). The spatial sub-division of the GSL in terms of phytoplankton abundance, as estimated from chlorophyll *a* concentration and productivity, has been already proposed by several research teams (de Lafontaine et al., 1991; Fuentes-Yaco et al., 1998; Lavoie et al., 2007) and for three periods of the year, spring, summer and fall. The classification schemes differ with respect to the number of clusters (e.g., 4 in de Lafontaine et al., 1991, 13 in Fuentes-Yaco et al., 1998), the attribute (e.g., chl in Fuentes-Yaco et al., 1998, phytoplankton productivity in de Lafontaine et al., 1991) and data (e.g., simulated in Lavoie et al., 2007, shipboard in de Lafontaine et al., 1991, and satellite-derived in Fuentes-Yaco et al., 1998) used to create the geographic segmentation. Likewise, the phytoplankton spatial trends identified by these studies do not always agree and major discrepancies have identified in the southern part of GSL during fall (Lafontaine et al., 1991; Lavoie et al., 2007).

Optical properties of GSL surface waters are influenced not only by phytoplankton variability but also by contributions derived from dissolved (e.g., CDOM) and particulate (e.g., sediments, detritus) components having a terrestrial origin (Nieke et al., 1997; Larouche and Boyer-Villemaire, 2005). These additional optical constituents are mainly supplied by advection of estuarine waters into the Gulf (Larouche, 1998), tributaries allocated in the northern shore of the GSL (Nieke et al., 1997), and topographically-driven resuspension over the shallow zones (Fuentes-Yaco et al., 1998). First studies describing optical properties of phytoplankton in the GSL were based on light absorption measurements (Roy et al., 1998) and highlighted the major impact of "packaging effects" on a_{ph} and a^*_{ph} variability.

2.2 Field measurements

The comparison of satellite and in situ measurements of chl and $a_{ph}(443)$ values was made based on two datasets corresponding to 17–30 May 2000 and 4–17 April 2001. In general for the GSL, spring is the most productive season of the year and coincides with a period of maximum illumination of the water column due to the higher sun altitude and the lower cloudiness (Montes-Hugo and Mohammadpour, 2013). Therefore, spring

is an ideal temporal window for performing remote sensing studies based on passive optical sensors. The location of the sampling locations during each cruise is plotted in Fig. 1. Based on Saint Lawrence River flow rates at Quebec City, May 2000 surveys in the GSL were influenced by a greater supply of freshwater discharge coming from Saint Lawrence Estuary ($1.6 \times 10^4\ m^3\ s^{-1}$) with respect to April 2001 ($1.4 \times 10^4\ m^3\ s^{-1}$) (Larouche and Boyer-Villemaire, 2010). Also, the sea ice cover during these cruises was absent or localized over small areas (e.g., Belle Strait and Northumberland Strait) (Saint Lawrence Global Observatory, http://ogsl.ca/).

During each oceanographic expedition, water samples for a_{ph} and chl were collected using a Rosette sampler equipped with 30 L bottles. In all cases, samples were obtained from water depths between 0.5 and 14 m or within the first optical depth previously computed from Secchi disk depth measurements. Vertical samples for each sampling location were binned using the arithmetic average (3 to 6 samples for chl, one sample at 1.5 m depth for a_{ph}). The protocol for a_{ph} measurements was based on the filter-pad technique (Mitchell et al., 2002) and is fully described by Roy et al. (2008). The coefficient of variation (i.e., CV = standard deviation/arithmetic average) of a_{ph} calculations as percentage is 17 %. Chlorophyll a determinations were performed based on HPLC (High Pressure Liquid Chromatography) analysis and following Zapata et al. (2000) technique (Roy et al., 2008). The analysis of chl based on this method has an average uncertainty of 10 %.

2.3 Satellite imagery

Ocean color daily images from SeaWiFS (Sea-viewing Wide Field-of-view Sensor) (L1, MLAC or merged local area coverage, footprint = 1.1 km) were obtained from NASA (The National Aeronautics and Space Administration, http://oceancolor.gsfc.nasa.gov/). Calibrated radiances at seven spectral bands (1: 402–422 nm, 2: 433–453 nm, 3: 480–500,nm, 4: 500–520 nm, 5: 545–565 nm, 6: 660–680 nm, 7: 745–785 nm, and 8: 845–885 nm) were derived from geo-referenced L1 scenes. Additional L2 products were extracted for evaluating different inversion models (a_{ph}(443)_Carder,

a_{ph}(443)_QAA, and a_{ph}(443)_GSM) (acronym definitions in Sect. 2.5 and Table 1). In all cases, the processing of satellite-derived values was conducted using the default a^*_{ph} curve implemented by SeaDAS (SeaWiFS Data Analysis System). This allowed to examine a posteriori the specific effect of natural variability of a^*_{ph} on satellite-based a_{ph} and chl estimates. Matching between satellite and field measurements was done within 6 h of the satellite overpass and using the median of valid data (i.e., positive values with a magnitude above the sensor sensitivity and below the sensor saturation, Tables 8 and 12 in Barnes et al., 1994) inside a mask of 3 × 3 pixels.

2.4 Atmospheric correction

Two atmospheric correction techniques were used: the standard SeaWiFS algorithm developed by Bailey et al. (2010) (hereafter SA) and the coupled ocean–atmosphere model proposed by Kuchinke et al. (2009) (hereafter KU). Notice that the notation NIR is used when operations involve both 765 and 865 nm wavelengths. The SA approach is an improvement of the atmospheric correction scheme originally suggested by Stumpf et al. (2003) and is based on updated look-up-tables (LUT) of aerosols parameterizations derived from the aerosol robotic network (Ahmad et al., 2010). Briefly, SA computation steps are summarized as follows: (1) calculation of a(670) based on a R_{rs}-based model of chl derived from the NOMAD dataset (Werdell and Bailey, 2005), (2) calculation of b_{bp}(670) from a(670) (Gordon et al., 1988), (3) extrapolation of b_{bp}(670) to NIR wavelengths using expression from Lee et al. (2010), (4) reconstruction of R_{rs}(NIR) from b_{bp}(NIR), (5) calculation of aerosol reflectance, and (6) iteration from 1 to 5 till convergence of R_{rs}(NIR). The SA approach has demonstrated to reduce negative values of R_{rs}(412) and R_{rs}(490) estimates as computed by the traditional technique of Gordon and Wang (1994) in 40 % and 100 %, respectively

The KU algorithm combines an atmospheric model composed by a simple aerosol model and GSM-based IOPs for estimating the reflectance attributed to aerosols and water from non-linear optimization of spectral signatures also known as SOA (spectral optimization algorithm) (Chomko and Gordon, 2001). Aerosols are simulated based

on Mie theory, a range of refractive index values, and particle size spectra following a Junge power-law distribution. Although simplified by one parameter, the aerosol model coupled with SOA can deal with absorbing aerosols having a terrestrial origin. In order to find the solution, the SOA repeats the next sequence of tasks till convergence of a cost function: (1) assumption of $\rho_a(\mathrm{NIR}) = \rho_{aw}(\mathrm{NIR})$, (2) elimination of water and oxygen absorption contributions from $\rho_{aw}(\mathrm{NIR})$, (3) calculation of aerosol parameters linked to composition, size and concentration, (4) calculation of transmission factor for NIR and according to viewing and illumination geometries, (5) calculation of unknown IOPs from GSM (chl, $a_{CDOM}(443)$ and $b_{bp}(443)$, Table 1) and based on SeaWiFS spectral bands within the visible range, (6) calculation of ρ_{aw} (NIR) based on GSM-derived IOPs, (7) utilization of TOA reflectance and ρ_{aw} to improve aerosol estimates, and (8) repetition of 2 to 7 till $\rho_w(865)$ falls below 0.0001.

2.5 Inversion modeling of IOPs

Three optical inversion models, one empirical (Carder et al., 2006, hereafter EC) and two semi-empirical (Lee et al., 2002, hereafter QAA; Garver and Siegel, 1997; Maritorena et al., 2002, hereafter GSM) were used to estimate $a_{ph}(443)$ based on the aforementioned atmospheric correction techniques. In all cases, the inversion is based on R_{rs} measurements within the visible spectral range (400–700 nm). The EC is related to the empirical portion of the inversion developed for MODIS (Moderate-resolution Imaging Spectroradiometer) (Carder et al., 1999) but modified to account for SeaWiFS spectral bands (i.e., centered wavelength 510 instead of 532 nm). Values of $a_{ph}(443)$ are computed based on $R_{rs}(488)/R_{rs}(551)$ and $R_{rs}(510)/R_{rs}(551)$ ratios or $\rho 35$ and $\rho 45$, respectively:

$$a_{ph}(443) = 10^{-1.189-1.133\rho 35-2.151\rho 35^2-0.775\rho 45+7.592\rho 45^2} \quad (5)$$

The RMSE of Eq. (5) as evaluated with field a_{ph} measurements (range = 0.003–0.8 m^{-1}) is 0.195 (Carder et al., 2006). The deconvolution of IOPs by the quasi-

analytical algorithm QAA is done as follows: (1) calculation of $a(\lambda_0)$ at a reference wavelength λ_0 (555 nm for SeaWiFS), (2) derivation of the light backscattering coefficient for particulates ($b_{bp}(\lambda_0)$), (3) computation of total (water + particulates) light backscattering coefficient (b_b) at other wavelengths previous quantification of its spectral behavior, (4) calculation of a values at wavelengths different from λ_0, (5) reconstruction of $a_{CDOM}(443)$ and a_{CDOM} spectral variability from a, a_w and R_{rs}, and (6) calculation of $a_{ph}(\lambda)$ values after subtracting $a_{CDOM}(\lambda)$ and a_w from $a(\lambda)$. The main equations used by the QAA model version 5 are described in Lee et al. (2009).

Based on NOMAD measurements (range = 0.003 and 2 m^{-1}) the RMSE of $a_{ph}(443)$ estimates using the QAAv5 is 0.257 (Lee, 2006).

The GSM decomposition of ocean color contributions due to phytoplankton encompasses three steps: (1) calculation of $b_{bp}(443)$, $a_{CDOM}(443)$ and chl based on 5 centered wavelengths (412, 443, 490, 510, and 555 nm) and optimization of the solution using an annealing method constrained by a cost function, (2) calculation of $a(440)$ from Eq. (3) and using computed $b_{bp}(443)$ values, and (3) retrieval of a_{ph} by multiplying chl by $a^*_{ph}(443)$. Notice that GSM and QAA inversions apply the same a_w values (Morel, 1974) and a_{CDOM} definition (i.e, CDOM also includes absorption due to detritus). Unlike QAA, the spectral slope of b_{bp} (1.0337) and a_{CDOM} ($S = 0.0206\,\mathrm{nm}^{-1}$) in GSM do not depend on R_{rs} ratios. The GSM model is operational for chl values greater than 0 and smaller than 100 $\mathrm{mg\,m}^{-3}$ or $0 < a_{ph}(443) < 5.82$. For oceanic waters, the GSM inversions of $a_{ph}(443)$ have a RMSE of 0.35 (Lee, 2006). These uncertainties are anticipated to be greater in coastal waters having large values of a and/or b_b.

2.6 Model performance metrics

The accuracy of each atmospheric correction model and water leaving radiance inversion technique for estimating $a_{ph}(443)$ was evaluated based on three indices, the root mean square error (RMSE), the relative bias as percentage (RB), the median of the absolute bias (MAB).

The RMSE can be described as follows:

$$\mathrm{RMSE} = \left\{ \sum_{m=1}^{M} \left(x_m^{\mathrm{sat}} - x_m^{\mathrm{ship}} \right)^2 / M \right\}^{0.5} \quad (6)$$

where, $m = 1, 2, \ldots, M$, with M equal to the number of match-ups, x^{sat} and x^{ship} are SeaWiFS-derived and in situ values of $a_{\mathrm{ph}}(443)$, respectively. The difference $x^{\mathrm{sat}} - x^{\mathrm{ship}}$ is abbreviated along the text as $a_{\mathrm{ph}}(443)^{\mathrm{sat}}$ bias.

The mathematical expression for RB as percentage is:

$$\mathrm{RB}\ (\%) = 100 \left| \left(x_m^{\mathrm{sat}} - x_m^{\mathrm{ship}} \right) / x_m^{\mathrm{ship}} \right| \quad (7)$$

For each algorithm, RB was also computed with respect to the range of in situ $a_{\mathrm{ph}}(443)$ values: low ($0 < x^{\mathrm{ship}} \leq 1/3$ max), intermediate ($1/3$ max $< x^{\mathrm{ship}} \leq 2/3$ max), and high ($2/3$ max $< x^{\mathrm{ship}} \leq$ max), where max is the maximum value per cruise. The largest RB for the low, intermediate and high interval of $a_{\mathrm{ph}}(443)$ values was symbolized as $\mathrm{RB_L}$, $\mathrm{RB_M}$ and $\mathrm{RB_H}$, respectively.

The MAB was computed as follows:

$$\mathrm{MAB} = \mathrm{median}(\boldsymbol{V}) \quad (8)$$

where $\boldsymbol{V}$ is a vector with M elements of $|(x_m^{\mathrm{sat}} - x_m^{\mathrm{ship}})|$.

Since RMSE, RB and MAB values are always positive, we also calculated the median of the $a_{\mathrm{ph}}(443)^{\mathrm{sat}}$ bias without eliminating the sign of the differences (MB). In terms of prediction accuracy, the best combination of atmosphere–ocean algorithms (i.e., atmosphere correction and inversion models) was that one presenting the smallest magnitude of RMSE. In case the minimum RMSE was comparable between two or more comparisons, the one having the smallest value of MAB decided which approach ranked first.

3 Results

3.1 In situ variability of $a_{\mathrm{ph}}(443)$

In general for the whole GSL, the median and the standard deviation of in situ $a_{\mathrm{ph}}(443)$ determinations were larger in April 2001 with respect to May 2000 (3.8 and 3.3-fold, respectively) (Fig. 2). For the same sampling locations, the magnitude of $a_{\mathrm{ph}}(443)$ changed up to 6.7-fold between surveys made during spring of different years (e.g., station 25, Fig. 1). By considering different hydrographic domains, the strongest variations on magnitude of $a_{\mathrm{ph}}(443)$ (up to 5.4-fold) commonly occurred over areas dominated by major gyres (Madeleine and Cape Breton Islands, sta. 21, 23 and 24; Belle Isle Strait, sta. 13, 15 and 16, Fig. A1).

3.2 Impact of atmospheric correction and inversion models on accuracy of satellite $a_{\mathrm{ph}}(443)$ estimates

The performance of SeaWiFS for estimating $a_{\mathrm{ph}}(443)$ in surface waters of the GSL differed with respect to the type of atmospheric correction algorithm and inversion model applied during the image processing (Fig. 2). Notice that the scales corresponding to the y-axis (i.e., magnitude of $a_{\mathrm{ph}}(443)$ coefficient) differ between years and atmospheric correction methods. Also, sampling locations having no matchups (e.g., sta. 5, 11 and 12 during April 2001) between satellite and field measurements are not shown.

In general, the ability of SeaWiFS for deriving meaningful geophysical values (i.e., no negatives and/or extremely large) of $a_{\mathrm{ph}}(443)$ was comparable between 2000 and 2001 surveys. Indeed for both oceanographic cruises, satellite retrievals of $a_{\mathrm{ph}}(443)$ were possible in 86 % of the cases. The lack of valid satellite-based $a_{\mathrm{ph}}(443)$ estimates was neither linked to a specific region as data gaps on satellite-derived products were either observed in southern (sta. 21, 23 and 24, Fig. 2a), central (sta. 27, Fig. 2b) or northern (sta. 6, Fig. 2b) areas of the GSL.

Despite of this, the number of pixels with reliable $a_{ph}(443)$ information was found to be specifically connected with the methods used to process the ocean color satellite images. In that regard, the atmospheric correction algorithm KU produced the maximum percentage (up to 100 % for April 2001) of pixels having valid $a_{ph}(443)$ estimates. The opposite was true (up to 61 % for April 2001) for the ocean color data analyzed with the SA technique. With respect to the type of optical inversion, the EC was the model with the highest retrieval rate (up to 92 % for April 2001). Conversely, satellite estimates of $a_{ph}(443)$ were less successful (up to 25 % valid values for April 2001) when the GSM model was utilized.

Overall for the two cruises, the RB per sampling location and expressed as percentage ranged between 0.5 and 420 % depending on the type of parameterization used to remove the atmospheric optical components, and the chosen approach to derive the inherent optical properties of the water. In general, the error in predicting $a_{ph}(443)$ during April 2001 (RMSE up to 0.219, MAB up to 0.090) was larger with respect to May 2000 (RMSE up to 0.053, MAB up to 0.018) (Table 2). In May 2000, several image processing techniques (SA-QAA, SA-GSM and KU-QAA, Fig. 2a and c, Table 2) had a comparable RMSE (0.013) for estimating $a_{ph}(443)$. However, it was KU-QAA the one having the smallest MAB among them (0.005). In April 2001, the performance of KU-EC for estimating $a_{ph}(443)$ (RMSE = 0.076, Table 2) was clearly superior with respect to the other techniques (Fig. 2b and d). For both cruises, the prediction of $a_{ph}(443)$ using the best modeling approach and SeaWiFS measurements was linked to an underestimation of field values (MB up to $-0.066\,m^{-1}$ during April 2001).

In general, RBs calculations suggested that large uncertainties were not specifically associated with the magnitude of $a_{ph}(443)$. Indeed, relative errors greater than 100 % were present at low (RB_L up to 420.3 %), intermediate (RB_M up to 433.8 %) or high (RB_H up to 335.1 %) values of $a_{ph}(443)$ depending on the atmospheric correction, inversion and sampling period (Table 2). The largest RB for individual locations was larger for SA (up to 433.8 %) with respect to KU retrievals (up to 151 %). Comparisons among inversions were less clear as QAA was the model producing the smallest (up to 72.1 %

in May 2000) and the largest (up to 420.3 % in April 2001) relative deviations. However, comparisons made by merging years and atmospheric corrections, and based on the proportion of samples having a relative bias smaller than 50 % indicated a greater accuracy of QAA (0.83) with respect to EC (0.66) and GSM (0.29).

Finding an exact spatio-temporal correspondence between field measurements and satellite estimates of a_{ph} is challenging in coastal waters where oceanographic conditions and subsequent biogeochemical properties may drastically change in minutes. These effects are examined in Fig. 3 for each sampling station and during May 2000. Notice that only spaceborne predictions derived from KU-QAA are shown. Preliminary results showed a decrease on RB per cruise of 3.4 % when the number of pixels used for performing the matchup is increased from one to nine. Despite this accuracy improvement, the 10 and 90 % percentiles of the Whisker box plots suggest the presence of outliers in 36.4 % of the samples (e.g., sta. 21, Fig. 3a). The aforementioned discrepancy was not clearly related to variations on time difference between SeaWiFS and field determinations of $a_{ph}(443)$ as large biases (i.e., > 0.1 or $< -0.1\,m^{-1}$) were either associated to relatively small (2.2 h) (e.g., sta. 4, April 2001) and large (5.3 h) (e.g., sta. 13, April 2001) temporal offsets (Fig. 3b). In general, the observed errors between satellite and shipboard $a_{ph}(443)$ measurements were neither substantially linked to geographic differences within the GSL. In fact, major mismatches were either found in the northeastern, central or southern sampling locations (e.g., sta. 13, 21 and 27). However, the largest uncertainties (up to 79.3 %) appeared to be frequently associated with areas where strong upwelling events have been commonly reported (e.g., sta. 21, Figs. 1, 3a and A1).

3.3 Regional variability of algorithms performance with respect to KU-QAA

Geographic changes on spaceborne $a_{ph}(443)$ estimates due to the use of different atmospheric correction techniques and inversion models are depicted over the GSL in Fig. 4. The comparison is only made for 21 May 2000 given the greater proportion of valid pixels during that date. In all cases, the resulting satellite retrievals of $a_{ph}(443)$

are mapped with respect to the magnitude of $a_{ph}(443)$ as calculated by applying the Kuchinke's atmospheric correction approach and the QAA parameterization.

In general, the standard atmospheric correction technique used by SeaDAS 7.0 software (i.e., SA) generated unbiased $a_{ph}(443)$ estimates with respect to the most accurate approach (i.e., $a_{ph}(443)^{SA\text{-}QAA}/a_{ph}(443)^{KU\text{-}QAA} = 1$) when satellite retrievals were obtained over waters far from the shore (Fig. 4a). Conversely, the largest positive deviations (> 4-fold overestimation) associated with SA estimates followed closely the contour of land and cloud pixels. The SA underestimation of $a_{ph}(443)$ values with respect to KU estimates was unusual and only detected near the mouth of Bay Chaleur and over waters coinciding with the Anticosti Gyre.

By applying the same reference atmospheric correction protocol (i.e., KU), the implementation of the empirical inversion algorithm suggested by Carder et al. (2006) led to a general overestimation of $a_{ph}(443)$ with respect to the QAA estimates and over the whole Gulf of Saint Lawrence (Fig. 4b). Commonly, the proportion $a_{ph}(443)^{KU\text{-}EC}/a_{ph}(443)^{KU\text{-}QAA}$ was greater than 1.16 for most of the waters far from the coastline. Despite the large horizontal variability, the maximum positive deviations (> 1.4) were frequently observed around the Madeleine Islands and NE of the Anticosti Island. The underestimation of $a_{ph}(443)^{KU\text{-}QAA}$(relative bias < 0.75) was typically found near the coast (e.g., around the Gaspé Peninsula, northern shore of Quebec) and inside several Bays in New Brunswick (e.g., Miramichi Estuary) and Newfoundland (e.g., St. Georges Bay) (Fig. 1).

In contrast with the above findings, the magnitude of $a_{ph}(443)$ was currently underestimated in 50 % with respect to the QAA values when the semi-empirical algorithm of GSM was used (Fig. 4c). The smallest $a_{ph}(443)^{KU\text{-}GSM}/a_{ph}(443)^{KU\text{-}QAA}$ values (< 0.2) were specifically situated south of the Prince Edward Island. Relative deviations with respect to KU-QAA of up to 70 % (i.e., ratios ∼ 0.3) were detected inside the Bay of Chaleur, along Gaspé Peninsula and waters extending NE to the central part of the GSL. Likewise, locations with anomalously small $a_{ph}(443)$ values derived from GSM were characteristic of waters north of the Anticosti Island. Conversely, the GSM inversion model rarely overestimated the $a_{ph}(443)$ estimates produced by the QAA model (e.g., Miramichi Estuary and St. Georges Bays).

3.4 Origin of satellite $a_{ph}(443)$ uncertainties

3.4.1 Variability of in situ a^*_{ph}

In average, the magnitude of shipboard measurements of $a_{ph}(443)$ normalized by the chlorophyll *a* concentration was greater in May 2000 (arithmetic mean ±2 standard errors, 0.0275 ± 0.0034 mg chlorophyll^{-1}m^2) with respect to April 2001 (0.0232 ± 0.0042 mg chlorophyll^{-1} m^2) (Fig. 5). As expected, most of the variability was observed around those wavelengths that are spectrally close to the absorption peaks of chlorophylls (i.e., 440 and 670 nm). The average spectral shape of $a^*_{ph}(443)$ sometimes revealed striking differences with respect to the default values implemented in SeaDAS. In May 2000, the $a^*_{ph}(443)$ measurements showed a good agreement (relative error < 5 %) with respect to those standard values proposed by NASA (Fig. 5a). However for April 2001, the arithmetic average of in situ $a^*_{ph}(443)$ was 42 % smaller with respect to SeaDAS default values (Fig. 5b). In general for the two surveys, the magnitude of $a^*_{ph}(670)$ used by SeaDAS underestimated (up to 48.3 %) the magnitude of *in-water* measurements. Conversely for the spectral range 550–650 nm, it was frequently found that default NASA values overestimated in situ a^*_{ph} determinations.

Regionally speaking, the horizontal variability of $a^*_{ph}(443)$ was associated with the geographic position of major hydrographic features of the Gulf of Saint Lawrence (Fig. A1). During May 2000, the smallest $a^*_{ph}(443)$ values were observed in waters coinciding with the flow of the Gaspé Current around the Gaspé Peninsula (sta. 1–3) and the largest anticlockwise gyres (e.g., west of Anticosti, sta. 5–8, and adjacent waters to Madeleine Islands, sta. 21–24) (Figs. 1 and A1 Table 3). Conversely, the magnitude of $a^*_{ph}(443)$ was frequently higher in surface waters corresponding to clockwise gyres (e.g., northwest of Madeleine Islands, sta. 17–20) and strong upwelling areas (e.g., southeast of the Anticosti Islands, sta. 25–28). In general, the aforementioned

relationships between $a^*_{ph}(443)$ and different hydrodynamic features were less clear in the GSL during spring of 2001 (Table 3), a year with a weaker freshwater discharge and stronger vertical mixing. A remarkable difference with respect to May 2000 was the inverse behavior of $a^*_{ph}(443)$ over the Anticosti gyre (sta. 5–8) and the upwelling zone north of the Anticosti Island (sta. 9–12).

Magnitude differences between in situ and SeaDAS default $a^*_{ph}(443)$ values had a major impact in remote sensing estimates of chl during the two cruises. Differences between in situ measurements as derived from HPLC and spaceborne chl estimates are summarized in Table 4 for the two cruises. Comparisons for May 2000 and April 2001 were performed based on KU-QAA and KU-EC approaches, respectively. In general, the use of SeaDAS default a^*_{ph} curves resulted in RB varying between 1.5 and 78.7 % for May 2000, and 19.3 and 88.5 % for April 2001. Satellite estimates based on realistic a^*_{ph} values had RBs ranging between 5.9 and 72.1 % for May 2000, and 8.3 and 81.0 % for April 2001. Based on the median RB per cruise, chl calculations using NASA standard a^*_{ph} values introduce an additional 3.4 % and 29.1 % error for May 2000 and April 2001 surveys, respectively. In terms of MAB, chl calculations using default SeaDAS a^*_{ph} introduced an additional uncertainty of 26 % and 50.8 % on spaceborne chl algorithms that were locally tuned with in situ a^*_{ph} measurements during May 2000 and April 2001 cruises, respectively.

4 Discussion

The seasonal and inter-annual variability of phytoplankton abundance in the GSL is characterized by large fluctuations due mainly to variations on river discharge, ice cover and wind patterns. These changing phytoplankton distributions have major implications on higher trophic levels of the GSL and adjacent oceanic waters. In fact, spatial and temporal changes on phytoplankton abundance inside the Gulf have an important influence on larvae survival of several commercial fisheries developing in the Scotian Shelf (e.g., northern shrimp and haddock) (Platt et al., 2003; Koeller et al., 2009). The aforementioned variability of phytoplankton and the large spatial extent of the GSL make unpractical the use of shipboard measurements for mapping phytoplankton distributions over the study region (Lavoie et al., 2007).

Here, satellite ocean color measurements are applied for deriving phytoplankton optical properties that are utilised a posteriori for computing horizontal chl fields over the GSL. As phytoplankton contribution to optical properties may dramatically vary between years, the use of general ocean color algorithms developed for oceanic waters may present large uncertainties in the GSL. To date, this issue has not been addressed by past (Fuentes-Yaco et al., 1997b, 1998) or contemporaneous (Le Fouest et al., 2005) investigations as their estimates were derived from standard biogeo-optical parameterizations (e.g., OC-4 polynomial model, NASA, O'Reilly et al., 1998) and atmospheric correction schemes (e.g., classic NIR-iterative aerosol correction from Gordon and Wang, 1994). Here, accuracy of two atmospheric correction methods and three inversion models were evaluated in the GSL for estimating $a_{ph}(443)$ and subsequent chl values based on SeaWiFS measurements.

4.1 In situ variability of a_{ph}

In general, our field measurements showed higher values of $a_{ph}(443)$ and lower values of $a^*_{ph}(443)$ during April 2001 with respect to May 2000. The greater magnitude of a_{ph} during April 2001 is in part related to the seasonal timing of the phytoplankton bloom in the GSL. During April, the sea ice cover is smaller with respect to March (Le Fouest et al., 2005). Also, the cloudiness is commonly reduced with respect to March and May (Montes-Hugo and Mohammadpour, 2013). Lastly, the supply of nutrients into the GSL is greater during April with respect to May (Lavoie et al., 2007). Thus, the phytoplankton growth is favored during April leading to an increase of a_{ph} associated with a greater synthesis of chlorophyll. Simulations using biological models coupled to hydrodynamics support our findings (Lavoie et al., 2007).

Larger accumulations of phytoplankton photosynthetic pigments and subsequent increase on $a_{ph}(443)$ and chl during April 2001 with respect to May 2000 was consistent

with the development of large-sized phytoplankton communities during 2001 (Roy et al., 2008). In fact and using a size index of phytoplankton assemblages based on diagnostic pigments, Roy et al. (2008) found that microphytoplankton contribution to the total chlorophyll *a* was 26 % greater in April 2001 with respect to May 2000.

Unlike $a_{ph}(443)$, $a^*_{ph}(443)$ measurements in the GSL followed an opposite trend between surveys with higher values during May 2000 with respect to April 2001. As pointed out by Roy et al. (2008), these changes can be attributed to variations on phytoplankton taxonomy and photo-physiology. Indeed, relatively high values of $a^*_{ph}(443)$ during May 2000 was determined by a greater abundance of small-sized cells, a greater production of photo-protective cells, and a smaller "packaging effect" associated with a stronger water stratification (see Sect. 4.2.5).

4.2 Spaceborne a_{ph} estimates

4.2.1 Atmospheric correction models

The Kuchinke et al. (2009) spectral optimization technique had the best overall performance to calculate $a_{ph}(443)$ among the atmospheric correction methods used in this study. In contrast, satellite-based $a_{ph}(443)$ estimates using Bailey et al. (2010) approach presented large deviations (up to 4-fold near the shore) with respect to in situ measurements. Although Bailey et al. (2010) includes more realistic aerosol distributions than those implemented by Kuchinke et al. (2009), the SA approach may be less accurate than KU due to two main reasons. First, SA computes $a(670)$ with a model constructed for case I waters (i.e., where IOPs variability only depend on phytoplankton concentration) (Gordon et al., 1988). Conversely, Kuchinke's algorithm operates with the semi-empirical GSM model, thus phytoplankton and CDOM contributions are independently parameterized and more accurate inversions can be obtained in optically complex waters like those investigated in the GSL. Second, γ or the spectral slope of b_b, is computed in SA based on $R_{rs}(443)/R_{rs}(555)$ (Lee et al., 2010), and may be associated to large prediction errors if *a* values are strongly influenced by CDOM

(e.g., May 2000 in the GSL). This is not occurring in KU since the magnitude of γ is derived from LUTs after optimization of a cost function. The above results also highlight the greater importance of changes on water optics with respect aerosol optical properties for deriving accurate a_{ph} estimates in our study area and during the period under investigation.

4.2.2 Inversion modeling of IOPs

Based on Kuchinke et al. (2009) atmospheric correction, the ability to estimate $a_{ph}(443)$ among different optical inversion models was evaluated. In general for optically complex waters, semi-empirical biogeo-optical models are expected to have a greater accuracy for estimating $a_{ph}(443)$ than empirical models. However, that was not the case in the GSL where empirical or semi-empirical approaches may represent the best option for predicting $a_{ph}(443)$ depending on the optical characteristics of the waters. During May 2000, the GSL was influenced by a greater inflow of optically complex waters coming from the Saint Lawrence Estuary and the QAA model was the technique presenting the smallest overall error (i.e., RMSE and MAB) for deriving $a_{ph}(443)$ values. Conversely for April 2001, GSL surface waters were characterized by a greater contribution from the Atlantic Ocean, and the EC model appeared as the best alternative for predicting the light absorbed by phytoplankton communities.

The advantage of using EC over QAA for estimating $a_{ph}(443)$ during April 2001 was probably apparent due to two causes. First, the empirical inversion suggested by Carder et al. (2005) is less able to separate covarying optical components with respect to QAA. Thus, part of the observed dependency between a_{ph} and R_{rs} ratios used by EC was attributed to non-algal optical contributions such as CDOM and detritus. Second, the measured chl values in the GSL during April 2001 were well above (1.76 to 8.46 $mg\,m^{-3}$) the working range of EC (up to 1.5 $mg\,m^{-3}$). Therefore, EC-derived $a_{ph}(443)$ estimates during April 2001 should be interpreted with caution.

A consistent pattern during the two surveys was the greater accuracy of KU-QAA with respect to KU-GSM calculations of $a_{ph}(443)$. This was attributed to differences

between inversion models in terms of spectral variability and a^*_{ph} parameterization. First, the error on $a_{ph}(443)$ estimates is anticipated to be greater in GSM calculations since $a_{ph}(443)$ values are derived by multiplying the simulated concentration of chlorophyll *a* by the $a^*_{ph}(443)$ as estimated by optimization of values obtained from LUT tables. The caveat in this approach is that two error terms coming from chl and $a^*_{ph}(443)$ are added every time that $a_{ph}(443)$ is estimated. Second, the LUT of $a^*_{ph}(\lambda)$ values available in SeaDAS and used by the GSM model may result in large deviations with respect to in situ values measured over the GSL. In a different way, the QAA computes $a_{ph}(443)$ by subtracting the CDOM and seawater contributions to the total *a* coefficient. In this case, the uncertainty on a_{ph} is mainly driven by a_{CDOM} + detritus estimates and does not rely on previously selected a^*_{ph} values. As later discussed in the text, the choice of site-specific a^*_{ph} values is critical for implementing accurate regional biogeo-optical models in the GSL.

4.2.3 Differences on satellite-derived a_{ph} uncertainties between surveys

Regardless of the atmospheric correction or inversion model under evaluation, the error on estimating $a_{ph}(443)$ based on spaceborne ocean color measurements was in general larger in April 2001 with respect to May 2000. The amplitude of the optical signal associated with phytoplankton and with respect to the background (i.e., signal/noise) did not appear to be the cause since chl values were consistently higher (7.8-fold, arithmetic mean) in April 2001 with respect to May 2000. This pigment difference led to a higher contribution of phytoplankton to the total light attenuation during April 2011 even though the lower $a^*_{ph}(443)$ during this period. Moreover, the $a_{ph}(443)/a(443)$ decrease due to the a greater dominance of other optical components (e.g., CDOM, detritus, sediments) was not observed during April 2001 (e.g. $a_{CDOM}(443)$, $\tilde{x} \pm$ se between 0 and 14 m depth, $0.230 \pm 0.024\,m^{-1}$, May 2000, $0.132 \pm 0.016\,m^{-1}$, April 2001, se = standard error). Thus, if modifications on underwater light fields between surveys did not seem to be a decisive factor explaining the large uncertainties of satellite a_{ph}

estimates, Why remote sensing predictions of $a_{ph}(443)$ during April 2001 had more error? A less intuitive answer can be found after comparing the spatial variability of chl between cruises. As reported above, in situ measurements of $a_{ph}(443)$ were more variable throughout the GSL and during April 2001 due to a greater spatio-temporal variability of chl values. Consequently, it would be not surprising to find a worst mismatch between field observations and satellite estimates of $a_{ph}(443)$ during April 2001. This spatial variability may also explain the lack of coherence between some satellite estimates and shipboard measurements depicted in Fig. 3. Future work should be focused in characterizing this spatial variability in order to improve the accuracy of spaceborne retrievals.

4.2.4 Geographic distribution of satellite-derived a_{ph} uncertainities

The ratio between SeaWiFS-derived $a_{ph}(443)$ estimates as computed from SA and KU algorithms and based on QAA inversion was very useful to delineate areas of the GSL where the standard atmospheric correction imbedded in SeaDAS may result in major biases for estimating a_{ph} and associated phytoplankton distributions in the GSL.

In general for 21 May 2000, SA-based calculations tended to overestimate KU (up to 5-fold) a_{ph} retrievals near the shore where a substantial resuspension of sediments is suspected to be the cause (e.g., the Northumberland Strait). The Northumberland Strait is part of the Magdalen Shallows, a shelf environment with an average depth of 50 m and with a water column highly influenced by wind and bottom stress mixing (De Lafontaine et al., 1991). Fuentes-Yaco et al. (1998) investigated the variability of phytoplankton chlorophyll in this region based on ocean color images obtained by the CZCS (Coastal Zone Color Scanner Sensor) between 1979 and 1981. Based on monthly satellite image composites, Fuentes-Yaco et al. (1998) detected during April several pixels presumably contaminated by optical contributions derived from suspended particulate matter. Also, they found during May higher phytoplankton pigment concentrations along the Northumberland Strait that were likely overestimated by the presence

of suspended sediments. In that regard, the CZCS has not NIR channels, thus the use of this imager over turbid waters is not reliable.

Deviations of SeaWiFS-based $a_{ph}(443)$ estimates derived from EC and GSM with respect to QAA model had different spatial patterns in the GSL. In general, EC overestimated QAA optical inversions over the whole study area even though major relative differences occurred toward the NE of the Gulf. During spring, this sub-region is characterized by low chlorophyll values (Lavoie et al., 2007). In addition, extra CDOM not associated to phytoplankton was present in the Gulf especially to the northern coast and during May 2000. Since EC retrievals are highly sensitive to CDOM contributions non-related to phytoplankton, the calculations of $a_{ph}(443)$ by EC and over these water parcels are anticipated to be highly overestimated with respect to those QAA estimates.

A close examination of spatial changes of satellite-derived $a_{ph}(443)$ ratios as derived from GSM and QAA models coupled to KU revealed an underestimation of GSM-based with respect to QAA-based $a_{ph}(443)$ calculations. These differences were more dramatic over zones of the GSL that are typically rich in suspended solids (e.g., Northumberland Strait, eastward of the Gaspé Peninsula) (Fuentes-Yaco et al., 1998; Lavoie et al., 2007). It is suggested that these GSM-related deviations with respect to QAA were likely related to the lack of regional tuning of GSM parameters describing the IOPs of particulate components. In particular, these changes were probably attributed to the bias on particulate backscattering properties since default a^*_{ph} values used by GSM inversions were comparable to those measured in situ during May 2000.

4.2.5 Error sources related to a^*_{ph}

The contribution of phytoplankton photo-acclimation to a_{ph} uncertainties varied between surveys and among locations for the same survey. In that regard, the photo-acclimation and pigment composition of phytoplankton were two major sources of error for estimating a_{ph} and chl from the space. Relative errors of up to 29.1 % (i.e., median RB per cruise) were associated to the use of SeaDAS default a^*_{ph} libraries. These biases were larger or smaller than those attributed to differences on atmospheric cor-

rection (up to 24.3 %) and optical inversion models (up to 43.4 %), respectively. Also, an additional issue for estimating $a_{ph}(443)$ arises when the magnitude of a^*_{ph} is relatively small. Relatively large a^*_{ph} values improve the accuracy of inversion models such as KU due to a greater signal associated with phytoplankton that creates a greater spectral variability on water reflectance (Kuchinke et al., 2009).

If field measurements of a^*_{ph} are not available in the area to be investigated, Can we simulate a^*_{ph} values without using global LUTs or unrealistic regional values? This important question still remains unanswered even though our results suggest two interesting approaches to understand and parameterize the spatial and temporal variability of a^*_{ph} at least in the GSL. In the first approach, the optical cross section of phytoplankton may be modeled as a function of abundance of photoprotective pigments, size distribution of cells, and PAR (photosynthetic available radiation) availability. Some relationships between a^*_{ph}, photoprotective pigments and size spectra of phytoplankton have been already elucidated by Roy et al. (2008) in the Saint Lawrence System who found lower values of a^*_{ph} during April 2001 linked to large-sized diatoms and a smaller proportion of photoprotective carotenoids. Although promising, this study was not able to separate the two primary variables affecting the a^*_{ph} magnitude and related to the "pigment packaging effect", the bulk size of the phytoplankton cells and the photo-acclimation state of those cells.

In the GSL, preliminary analysis showed a greater water column stratification, as computed from Sigma-t density differences between 0 and 60 m depth, during May 2000 (1.66 ± 0.53 Kg m^{-3}) with respect to April 2001 (0.82 ± 0.41 Kg m^{-3}). These conditions supports the idea that low values of a^*_{ph} during April 2001 with respect to May 2000 were also related to a greater dominance of shade-adapted phytoplankton communities during the first period. This indicates that not only size structure and pigment composition of microalgae are important factors altering a^*_{ph} in the GSL but also the adaptation of phytoplankton cells to different light levels. In the second approach, it is suggested that time and space changes of a^*_{ph} can be potentially modeled based on geo-statistical relationships between a^*_{ph} and hydrographic features. Indeed

in our study, we found that relatively high or low a^*_{ph} values are preferentially associated with different eddy spinning directions and strength of vertical current velocities as inferred from regional differences on upwelling intensity. Also, it was deducted that these bio-physical linkages varied between years having different river discharge and water stratification.

5 Concluding remarks

The optimum selection of atmospheric correction techniques and optical inversion models is fundamental for deriving accurate IOPs from satellite-based ocean color data. In this study, the Kuchinke et al. (2009) atmospheric correction algorithm proved to be the most suitable choice for predicting $a_{ph}(443)$ values over the GSL and based on remote sensing reflectance measurements obtained from visible and NIR channels of SeaWiFS. The preference of using QAA or EC inversion methods was related to the optical complexity of the water confirming the initial hypothesis of this contribution. An essential parameter for obtaining accurate estimates of a_{ph} and chl in GSL waters was the optical cross section of phytoplankton light absorption. Our datasets suggest that ignoring a^*_{ph} variability may result in satellite-derived chl uncertainties (up to 29 %) that are larger or smaller than errors originated from atmospheric correction (up to 24.3 %) and inversion of IOPs (up to 43.4 %), respectively.

Acknowledgements. The authors thank to reviewers for their helpful suggestions. Likewise, we are in debt with Suzanne Roy at ISMER for sharing field data collected during May 2000 and April 2001 cruises. This is a contribution of the research project OSPLE (Optical remote sensing models for estimating suspended particulate matter in the St. Lawrence Estuary) awarded to M. Montes-Hugo and supported by NSERC (Natural Sciences and Engineering Research Council of Canada).

References

Ahmad, Z., Franz, B. A., McClain, C. R., Kwiatkowska, E. J., Werdell, J., and Shettle, E. P.: New aerosol models for the retrieval of aerosol optical thickness and normalized water-leaving radiances from the SeaWiFS and MODIS sensors overcoastal regions and open oceans, Appl. Optics, 49, 5545–5560, 2010.

Bailey, S. W., Franz, B. A., and Werdell, P. J.: Estimation of near-infrared water-leaving reflectance for satellite ocean color data processing, Opt. Express, 18, 7521–7527, 2010.

Balch, W. M., Eppley, R. W., Abbott, M. R., and Reid, F. M. H.: Bias in satellite-derived pigment measurement due to coccolithophores and dinoflagellates, J. Plankton Res., 11, 575–581, 1989.

Barnes, R. A., Holmes, A. W., Barnes, W. L., Esaias, W. E., McClain, C. R., and Svitek, T.: SeaWiFS prelaunch radiometric calibration and spectral characterization, in: SeaWiFS Technical Report Series, edited by: Hooker, S. B., Firestone, E., R., and Acker, J. G., NASA Technical Memorandum, NASA Goddard Space Flight Center, Greenbelt, Maryland, 104566, vol. 23, 55 pp., 1994.

Bricaud, A., Claustre, H., Ras, J., and Oubelkheir, K.: Natural variability of phytoplankton absorption in oceanic waters: influence of the size structure of algal populations, J. Geophys. Res., 109, 1–12, doi:10.1029/2004JC002419, 2004.

Carder, K. L., Chen, F. R., Lee, Z. P., and Hawes, S. K.: Semianalytical moderate-resolution imaging spectrometer algorithms for chlorophyll *a* and absorption with bio-optical domains based on nitrate-depletion temperatures, J. Geophys. Res., 104, 5403–5421, 1999.

Carder, K. L., Canizzaro, J. P., Chen, F. R., and Lee, Z. P.: MODIS semi-analytical algorithm for IOps, in: Remote Sensing of Inherent Optical Properties: Fundamentals, Test of Algorithms and Applications, edited by: Zhong Ping Lee, Chapter 9, International Ocean Color Coordinating Group, Report 5, Dartmouth, Canada, 63–67, 2006.

Charlson, R. J., Lovelock, J. E., Andrea, M. O., and Warren, S. G.: Oceanic phytoplankton, atmospheric sulphur, cloud albedo and climate, Nature, 326, 655–661, 1987.

Chomko, R. M. and Gordon, H. R.: Atmospheric correction of ocean color imagery: test of the spectral optimization algorithm with the sea-viewing wide field-of-view sensor, Appl. Optics, 40, 2973–2984, 2001.

de Lafontaine, Y., Demers, S., and Runge, J. A.: Pelagic food-web interactions and productivity in the Gulf of St. Lawrence: a perspective, in: The Gulf of St. Lawrence: Small Ocean or

Big Estuary?, edited by: Therriault, J.-C., Can. Spec. Publ. Fish. Aquat. Sci., 113, Dep. of Fisheries and Oceans, Ottawa, Ont., Canada, 99–123, 1991.
Fuentes-Yaco, C., Vezina, A. F., Gosselin, M., Gratton, Y., and Larouche, P.: Influence of late summer storms on the horizontal variability of phytoplankton pigment determined by Coastal Zone Color Scanner images in the Gulf of St. Lawrence, edited by: Ackleson, S., Proc. SPIE Vol. 2963, Ocean Optics XIII, 678–683, 1997a.
Fuentes-Yaco, C., Vezina, A. F., Larouche, P., Vigneau, C., Gosselin, M., and Levasseur, M.: Phytoplankton pigment in the Gulf of St. Lawrence, Canada, as determined by the coastal zone color scanner – Part I: spatio-temporal variability, Cont. Shelf Res., 17, 1421–1439, 1997b.
Fuentes-Yaco, C., Vezina, A. F., Platt, T., Harrison, W. G., Cormier, P. G., Wait, L. E., and Devine, L.: Spatio-temporal distribution of phytoplankton pigments in Northumberland Strait: CZCS imagery and in situ data, Canadian Technical Report of Hydrography and Ocean Sciences No. 195, 1998.
Garver, S. A. and Siegel, D. A.: Inherent optical property inversion of ocean colorspectra and its biogeochemical interpretation: 1 time series from the Sargasso Sea, J. Geophys. Res., 102, 18607–18625, 1997.
Gilerson, A., Gitelson, A., Zhou, J., Gurlin, D., Moses, W., Ioannou, I., and Samir, A.: Algorithms for remote estimation of chlorophyll *a* in coastal and inland waters using red and near infrared bands. Opt. Express, 18109–24125, 2010.
Gordon, H. R. and McCluney, W. R.: Estimation of the depth of sunlight penetrationin the sea for remote sensing, Appl. Optics, 14, 413–416, 1975.
Gordon, H. R. and Wang, W.: Retrieval of water-leaving radiance and aerosol optical thickness over the oceans with SeaWiFS: a preliminary algorithm, Appl. Optics, 33, 443–452, 1994.
Gordon, H. R., Brown, O. B. R., Evans, H., Brown, J. W., Smith, R. C., Baker, K. S., and Clark, D. K.: A semianalytic radiance model of ocean color, J. Geophys. Res., 93, 10909–10924, 1988.
Josenhans, H.: Atlas of the marine environment and seabed geology of the Gulf of St. Lawrence, Geological Survey of Canada, Open File 5346, 142 pp., doi:10.4095222864, 2007.
Koeller, P., Friedland, K., Fuentes-Yaco, C., Han, G., Kulka, D., O'Reilly, J., Platt, T., Richards, A., and Taylor, M.: Remote sensing applications in Stock assesments, in: IOCCG Report 8:

Remote Sensing in Fisheries and Aquaculture, Chapter 3, edited by: Forget, M.-H., Stuart, V., and Platt, T., 120 pp., 29–42, 2009.
Koutitonsky, V. G. and Budgen, G. L.: The physical oceanographyof the gulf of St. Lawrence: a review with emphasis on thesynoptic variability of the motion, in: The Gulf of St. Lawrence: Small Ocean or Big Estuary?, edited by: Therriault, J.-C., Can. Spec. Publ. Fish. Aquat. Sci., vol. 113, 57–90, 1991.
Kuchinke, C. P., Gordon, H. R., Harding Jr., L. W., and Voss, K. J.: Spectral optimization for constituent retrieval in case 2 waters I: Implementation and performance, Remote Sens. Environ., 113, 571–587, 2009.
Larouche, P.: SeaWIFS validation program in the St. Lawrence Estuary and Gulf, Fifth International Conference on Remote Sensing for Marine and Coastal Environments, San Diego, California, 5–7 October, 349–359, 1998.
Larouche, P. and Boyer-Villemaire, U.: Suspended particulate matter in the St. Lawrence Estuary and Gulf surface layer and development of a remote sensing algorithm, Estuar. Coast. Shelf S., 90, 241–249, doi:10.1016/j.ecss.2010.09.005, 2010.
Lavoie, D., Starr, M., Zakardjian, B., and Larouche, P.: Identification of ecologically and biologically significant areas (EBSA) in the Estuary and Gulf of St. Lawrence: primary production, Research Doc. 2007/079, Canadian Science Advisory Secretariat, 2007.
Le Fouest, V., Zakardjian, B. F., Saucier, J., and Starr, M.: Seasonal versus synoptic variability in planktonic production in a high-latitude marginal sea: the Gulf of St. Lawrence (Canada), J. Geophys. Res., 110, C09012, 2005.
Lee, Z. P.: Remote sensing of inherent optical properties: fundamentals, test of algorithms and applications, Report 5, edited by: Zhong Ping Lee International Ocean Color Coordinating Group, 126 pp., 2006.
Lee, Z. P., Carder, K. L., and Arnone, R. A.: Deriving inherent optical properties from water color: a multi-band quasi-analytical algorithm for optically deep waters, Appl. Optics, 41, 5755–5772, 2002.
Lee, Z. P., Arnone, R. A., Hu, C. Werdell, P. J., and Lubac, B.: Uncertainties of optical parameters and their propagations in an analytical ocean color inversion algorithm, Appl. Optics, 49, 369–381, 2010.
Levender, S. J., Pinkerton, M. H., Moore, G. F., Aiken, J., and Blondeau-Patissier, D.: Modification to the atmospheric correction of SeaWiFS ocean colour imagesover turbid waters, Cont. Shelf Res., 25, 529–555, 2005.

Maritonera, S., Siegel, D. A., and Peterson, A. R.: Optimization of semianalytical ocean color model for global scale applications, Appl. Optics, 41, 2705–2714, 2002.
Mitchell, B. G., Kahru, M., Wieland, J., and Stramska, M.: Determination of spectral absorption coefficients of particles, dissolved material and phytoplankton for discrete water samples, in: Ocean Optics Protocols for Satellite Ocean Color Sensor Validation, Revision 3, edited by: Mueller, J. L. and Fargion, G. S., NASA Technical Memorandum, 2002-21004/Rev 3, vol. 2, NASA Goddard Space Center, Greenbelt, Maryland, 231–257, 2002.
Montes-Hugo. M. and Mohammadpour, G.: Satellite-derived suspended particulates in the Saint Lawrence Estuary: uncertainties due to bottom effects, Can. J. Remote Sens., 34, 444–454, 2013.
Montes-Hugo, M., Carder, K., Foy, R., Cannizzaro, J., Brown, E., and Pegau, S.: Estimating phytoplankton biomass in coastal waters of Alaska using airborne remote sensing, Remote Sens. Environ., 98, 481–493, 2005.
Morel, A. and Antoine, D.: Heating rate within the upper ocean in relation to its bio-optical state, J. Phys. Oceanogr., 24, 1652–1665, 1994.
Morel, A., Antoine, D., and Gentili, B.: Bidirectional reflectance of oceanic waters: accounting for Raman emission and varying particle scattering phase function, Appl. Optics, 41, 6289–6306, 2002.
Nieke, B., Reuter, R., Heuermann, R., Wang, H., Babin, M., and Therriault, J.-C.: Light absorption and fluorescence properties of chromophoric dissolved organic matter (CDOM) in the St. Lawrence Estuary (Case 2 waters), Cont. Shelf Res., 17, 235–252, 1997.
O'Reilly, J. E., Maritorena, S., Mitchell, B. G., Siegel, D. A., Carder, K. L., and Garver, S. A.: Ocean color chlorophyll algorithms for SeaWiFS, J. Geophys. Res., 103, 24937–24953, 1998.
Platt, T., Fuentes-Yaco, C., and Frank, K. T.: Marine ecology: spring algal bloom and larval fish survival, Nature, 423, 398–399, 2003.
Roy, S., Blouin, F., Jacques, A., and Therriault, J. C.: Absoprtion properties of phytoplankton in the Lower Estuary and Gulf of St. Lawrence (Canada), Can. J. Fish. Aquat. Sci., 65, 1721–1737, 2008.
Runge, J. A., Castonguay, M., de Lafontaine, Y., Ringuette, M., and Beaulieu, J. L.: Covariation in climate, zooplankton, biomass and mackerel recruitment in the southern Gulf of St. Lawrence, Fish. Oceanogr., 8, 139–149, 1999.

Saucier, F. J., Roy, F., Gilbert, D., Pellerin, P., and Ritchie, H.: Modelling the formation and circulation processes of water masses and sea ice in the Gulf of St. Lawrence, Canada, J. Geophys. Res.-Oceans, 108, 1–20, 2003.
Savenkoff, C., Vézina, A. F., Smith, P. C., and Han, G.: Summer transports of nutrients in the Gulf of St. Lawrence estimated by inverse modelling, Estuar. Coast. Shelf S., 52, 565–587, 2001.
Stumpf, R. P., Arnone, R. A., Gould, R. W., Martinolich, P. M., and Ransibrahmanakul, V. A.: Partially-coupled ocean-atmosphere model for retrieval of water-leaving radiance from SeaWiFS in coastal waters, NASA/TM-2003-206892, vol. 22, edited by: Hooker, S. B. and Firestone, E. R., NASA Goddard Space Flight Center, Greenbelt, Maryland, 51–59, 2003.
Werdell, P. J. and Bailey, S. W.: An improved in-situ bio-optical data set for ocean color algorithm development and satellite data product validation, Remote Sens. Environ., 98, 122–140, 2005.
Wozniak, S. B. and Stramski, D.: Modeling the optical properties of mineral particles suspended in seawater and their influence on ocean reflectance and chlorophyll estimation from remote sensing algorithms, Appl. Optics, 43, 3489–3503, 2004.
Zapata, M., Rodriguez, F., and Garrido, J. L.: Separation of chlorophylls and carotenoids from marine phytoplankton: a new HPLC method using a reversed phase C8 column and pyridine-containing mobile phases, Mar. Ecol.-Prog. Ser., 195, 29–45, doi:10.3354/meps195029, 2000.

Table 1. List of acronyms.

Abbreviation	Definition	Units
a	total absorption coefficient	m^{-1}
b_b	total backscattering coefficient	m^{-1}
b_{bp}	backscattering coefficient of particulates	m^{-1}
a_w	absorption coefficient of seawater	m^{-1}
a_{ph}	absorption coefficient of phytoplankton	m^{-1}
a_{ph}^{sat}	SeaWiFS-derived a_{ph}	m^{-1}
a_{ph}^{ship}	ship-based a_{ph} determination	m^{-1}
$a_{ph}(443)^{sat}$ bias	$a_{ph}(443)^{sat} - a_{ph}(443)^{ship}$	m^{-1}
a_{ph}(443)_Carder	a_{ph} computed from Carder et al. (2009) empirical algorithm	m^{-1}
a_{ph}(443)_QAA	a_{ph} computed from Lee et al. (2002) quasi-analytical algorithm	m^{-1}
a_{ph}(443)_GSM	a_{ph} computed from Garver and Siegel (1997) and Maritorena et al. (2002) semi-empirical algorithm	m^{-1}
a_{ph}^{*}	specific absorption coefficient of phytoplankton	$m^2\,mg^{-1}$
chl	chlorophyll *a* concentration	$mg\,m^{-3}$
a_d	absorption coefficient of detritus	m^{-1}
a_{CDOM}	absorption coefficient of chromophoric dissolved organic matter	m^{-1}
nL_w	normalized water leaving radiance	$\mu W\,cm^{-2}\,sr^{-1}\,nm^{-1}$
L_a	radiance attributed to aerosols	$\mu W\,cm^{-2}\,sr^{-1}\,nm^{-1}$
t_{a-w}	air–water transmission factor	dimensionless
F_o	extraterrestrial solar irradiance	$\mu W\,cm^{-2}\,nm^{-1}$
R_{rs}	remote sensing reflectance	sr^{-1}
$\rho_a(\lambda)$	aerosol reflectance at wavelength λ	dimensionless
ρ_{aw}	aerosol + water reflectance	dimensionless
ρ_w	water reflectance	dimensionless

Table 2. Uncertainties on spaceborne a_{ph}(443) estimates. Acronyms SA, KU, QAA, EC, GSM, RMSE, MAB, MB, RB_L, RB_M and RB_H are defined in methods, nv is no valid satellite estimates, *n* is the number of observations.

Cruise			RMSE	MAB	MB	RB_L	RB_M	RB_H	*n*
2000	SA	EC	0.053	0.013	0.013	379.1	433.8	33.7	12
		QAA	0.013	0.012	−0.009	31.2	60.3	nv	8
		GSM	0.013	0.012	−0.008	86.7	27.6	nv	4
	KU	EC	0.014	0.010	0.009	151.0	51.0	33.1	10
		QAA	0.013	0.005	−0.004	72.1	29.3	52.9	10
		GSM	0.023	0.018	−0.018	61.2	67.9	75.6	10
2001	SA	EC	0.219	0.041	−0.006	59.9	39.3	335.1	12
		QAA	0.148	0.038	−0.021	420.3	103.4	87.3	8
		GSM	0.099	0.092	0.006	85.7	94.8	93.8	3
	KU	EC	0.076	0.066	−0.061	11.5	81.0	70.7	12
		QAA	0.100	0.070	−0.066	44.3	61.7	93.7	12
		GSM	0.114	0.095	−0.088	90.0	75.7	97.3	12

Table 3. Spatial distribution of $a^*_{ph}(443)$ in surface waters of the GSL. The median of $a^*_{ph}(443)$ ($a^*_{ph}(443)^{median}$) is computed for each cruise. Sampling locations are depicted in Fig. 1.

Sampling location	Hydrographic feature	($a^*_{ph}(443) - a^*_{ph}(443)^{median}$) May 2000	Apr 2001
1	Gaspé Current	−0.033	0.027
2	Gaspé Current	−0.048	−0.041
3	Gaspé Current	−0.046	−0.041
4	Anticosti Gyre	0.019	0.000
5	Anticosti Gyre	−0.034	0.014
6	Anticosti Gyre	−0.064	−0.002
7	Anticosti Gyre	−0.064	0.017
8	Anticosti Gyre	−0.045	0.017
9	North Anticosti Island	0.025	−0.024
10	North Anticosti Island	0.023	−0.017
11	North Anticosti Island	0.005	−0.010
12	North Anticosti Island	0.015	−0.041
13	Belle Isle Strait	0.010	−0.041
14	Belle Isle Strait	0.006	−0.041
15	Belle Isle Strait	0.016	−0.041
16	Belle Isle Strait	0.024	−0.041
17	Northwest Madeleine Islands Gyre	−0.016	0.007
18	Northwest Madeleine Islands Gyre	0.004	−0.025
19	Northwest Madeleine Islands Gyre	−0.008	−0.041
20	Northwest Madeleine Islands Gyre	−0.001	−0.026
21	Madeleine Islands Gyre	−0.034	−0.041
22	Madeleine Islands Gyre	−0.022	−0.041
23	Madeleine Islands Gyre	−0.025	−0.041
24	Madeleine Islands Gyre	−0.006	−0.041
25	Central Gulf Southeast Anticosti Island	0.001	0.008
26	Central Gulf Southeast Anticosti Island	0.029	−0.041
27	Central Gulf Southeast Anticosti Island	−0.002	−0.008
28	Central Gulf Southeast Anticosti Island	0.029	0.040

Table 4. Uncertainities on spaceborne chlorophyll estimates due to changes on $a^*_{ph}(443)$. chl^{HPLC} is the chlorophyll *a* concentration as derived from HPLC, dchl is the RB as percentage between chl^{HPLC} and SeaWiFS-derived chl values computed based on SeaDAS-default (superscript 1) and in situ measurements (superscript 2) of a^*_{ph}.

Sampling location	May 2000 chl^{HPLC} (mg m^{-3})	$dchl^1$ (%)	$dchl^2$ (%)	Apr 2001 chl^{HPLC} (mg m^{-3})	$dchl^1$ (%)	$dchl^2$ (%)
1				1.76	21.9	10.1
2						
3						
4				5.41	19.3	81.0
5						
6				7.55	69.0	34.8
7				6.43	73.4	47.0
8						
9				8.46	88.2	52.5
10				5.11	83.2	48.8
11						
12						
13	0.56	17.1	29.3	5.44	83.9	70.7
14	0.43	1.5	8.7			
15	0.46	14.9	7.7	3.97	85.0	8.3
16	0.38	16.0	16.7	5.45	88.5	63.1
17						
18						
19						
20						
21	2.65	78.7	52.9			
22						
23	1.01	33.3	7.6			
24	0.39	413.7	458.9			
25	0.40	3.2	5.9	6.58	80.9	54.7
26	0.49	21.7	14.0			
27	0.31	65.7	72.1	4.41	69.2	11.5
28	0.48	20.4	16.8	6.51	78.7	60.3

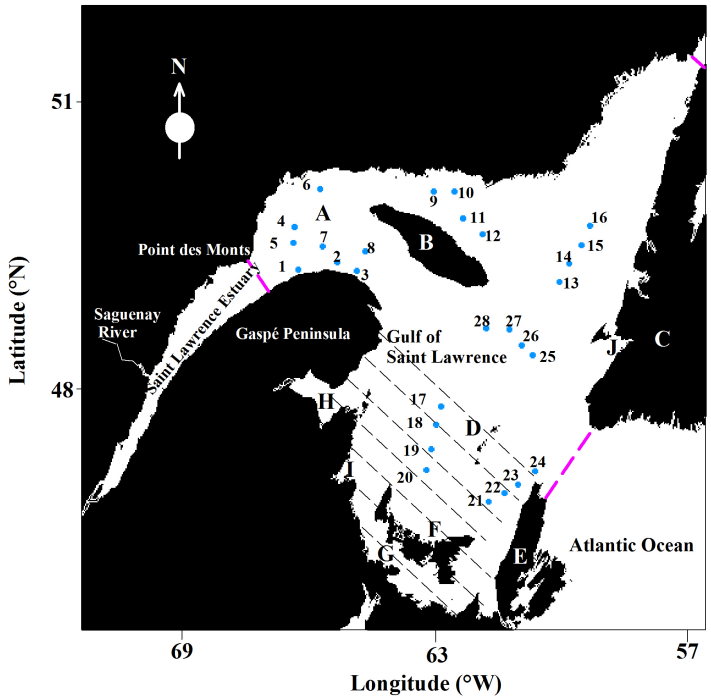

Figure 1. Study area. A. Anticosti Gyre, B. Anticosti Island, C. Newfoundland Island, D. Madeleine Islands, E. Cape Breton Island, F. Prince Edward Island, G. Northumberland Strait, H. Chaleur Bay, I. Miramichi Estuary, and J. St. Georges Bay. Sampling locations represented with numbers between 1 and 28, Magdalen shallows (hatched area). The western (Point des Monts), northern (Belle Isle Strait) and southern (Cabot Strait) boundaries of the Gulf of Saint Lawrence (Saucier et al., 2003) are indicated (broken magenta lines).

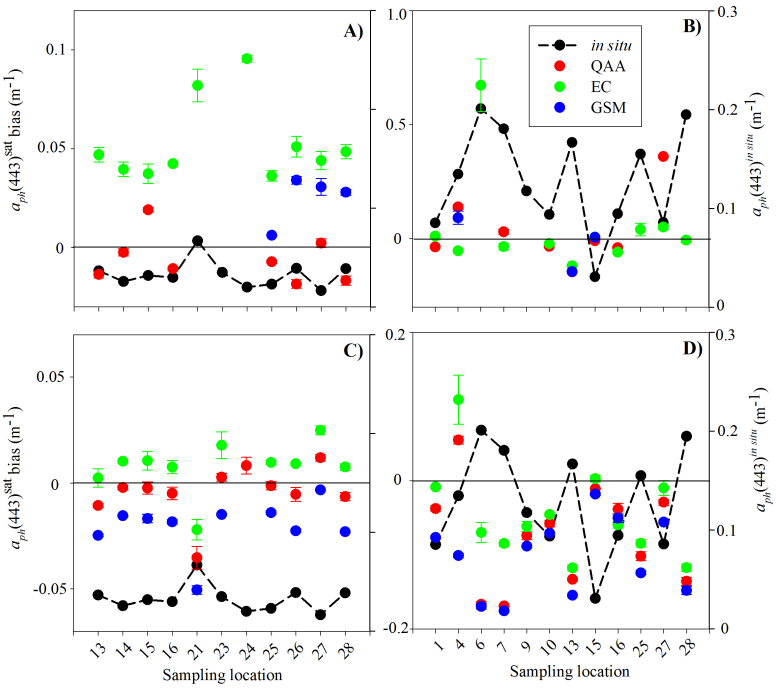

Figure 2. (A–D) Variability of satellite-derived and in situ measurements of $a_{ph}(443)$. Satellite retrievals for May 2000 **(A, C)** and April 2001 **(B, D)** cruises (left y-axis), atmospheric correction SA (upper panels) and KU (lower panels), field data (dash line and solid black circles, right y-axis), the horizontal line indicates no bias. Optical inversions with negative values are not shown, error bars correspond to two standard errors, SA, KU, QAA, EC, and GSM acronyms are defined in methods.

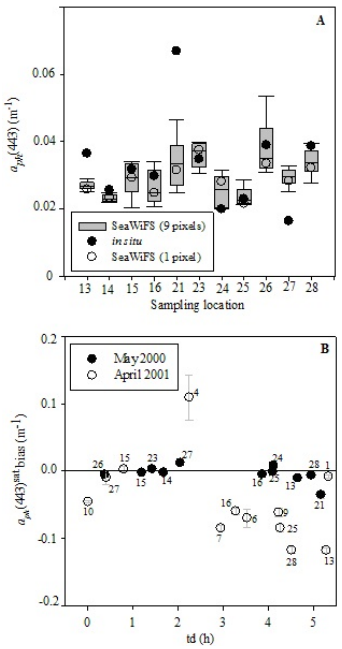

Figure 3. (**A** and **B**) Influence of space and time scales on matching satellite and in situ $a_{ph}(443)$ values. Comparison between satellite single (solid circle) nd multiple (Whisker bar) pixels estimates and field data (empty circles) **(A)**, KU-QAA estimates correspond to May 2000, each Whisker plot has a median (horizontal line) and bounding percentiles (10 and 90 %) (vertical dispersion limits). $a_{ph}(443)^{sat}$ bias as a function of time lag between satellite and in situ measurements (td) **(B)**, May 2000 and April 2001 satellite estimates correspond to KU-QAA and KU-EC models, respectively; no bias (solid horizontal line), name of sampling locations are indicated with numbers next to symbols. Error bars symbolize two standard errors.

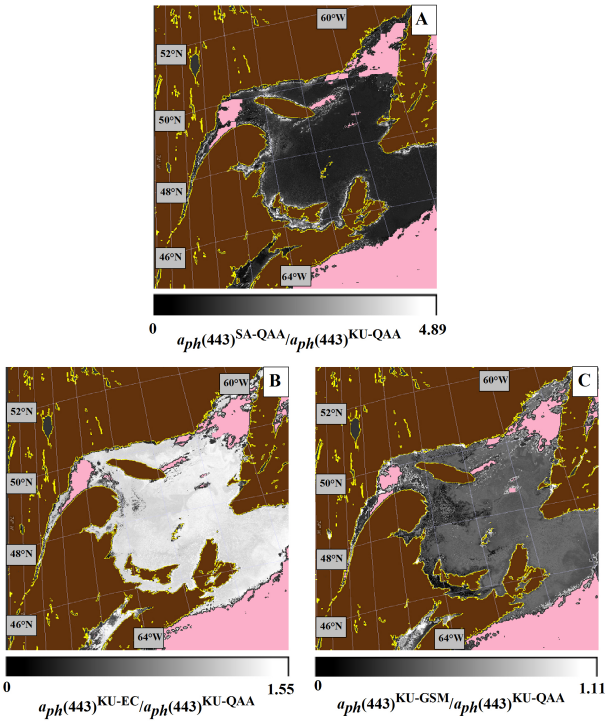

Figure 4. (A–C) Geographic variability of satellite-derived $a_{ph}(443)$ estimates with respect to KU-QAA predictions. All pixel-to-pixel ratios correspond to 21 May 2000. Deviations due to different atmospheric correction techniques **(A)** and optical inversion models **(B, C)**. Clouds are masked in pink, the grey scale of each plot is linear. SA, KU, QAA, EC, and GSM acronyms are defined in methods.

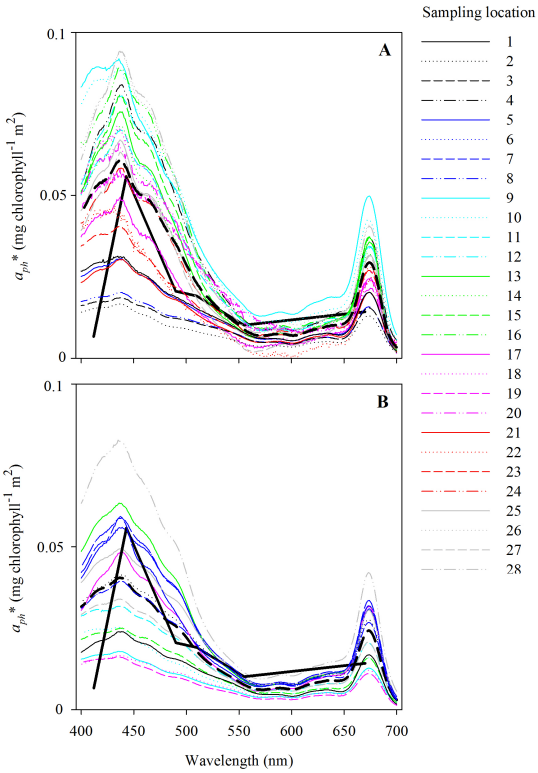

Figure 5. (**A** and **B**) Spectral behaviour of measured a^*_{ph}. May 2000 **(A)**, April 2001 **(B)**. Numbers represent sampling stations shown in Fig. 1. Arithmetic mean for each cruise (thick dash line), SeaDAS default (thick solid line). Each GSL sub-region is indicated with different colors and described in Table 3.

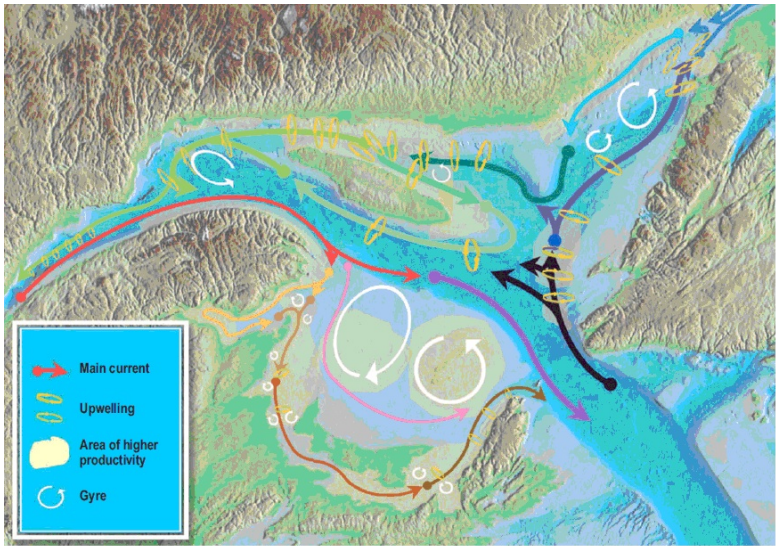

Figure A1. Circulation patterns in the Gulf of Saint Lawrence as drawn by Josenhans (2007).